Journal of Mechanical Design. Received May 31, 2021;
Accepted manuscript posted September 01, 2021. doi:10.1115/1.4052443

Development and validation of an end-effector for mitigation of collisions

Domenico Tommasino
Department of Industrial Engineering
University of Padova
Email: domenico.tommasino@phd.unipd.it

Matteo Bottin
Department of Industrial Engineering
University of Padova
Email: matteo.bottin@unipd.it

Giulio Cipriani
Department of Industrial Engineering
University of Padova
Email: giulio.cipriani@phd.unipd.it

Alberto Doria
Department of Industrial Engineering
University of Padova
Email: alberto.doria@unipd.it

Giulio Rosati
Department of Industrial Engineering
University of Padova
Email: giulio.rosati@unipd.it

In robotics the risk of collisions is present both in industrial applications and in remote handling. If a collision occurs, the impact may damage both the robot and external equipment, which may result in successive imprecise robot tasks or line stops, reducing robot efficiency. As a result, appropriate collision avoidance algorithms should be used or, if it is not possible, the robot must be able to react to impacts reducing the contact forces. For this purpose, this paper focuses on the development of a special end-effector that can withstand impacts. It is able to protect the robot from impulsive forces caused by collisions of the end-effector, but it has no effect on possible collisions between the links and obstacles. The novel end-effector is based on a bi-stable mechanism that decouples the dynamics of the end-effector from the dynamics of the robot. The intrinsically non-linear behavior of the end-effector is investigated with the aid of numerical simulations. The effect of design parameters and operating conditions are analyzed and the interaction between the functioning of the bi-stable mechanism and the control system is studied. In particular, the effect of the mechanism in different scenarios characterized by different robot velocities is shown. Results of numerical simulations assess the validity of the proposed end-effector, which can lead to large reductions in impact forces. Numerical results are validated by means of specific laboratory tests.

Nomenclature

x_c coordinate of the movement imposed by the robot control system.
x_r actual position of the robot mass.
k_r reduced stiffness of the robot.
c_r reduced damping coefficient of the robot.
m_r reduced mass of the robot.
F_b component of the force generated by the bi-stable mechanism in the sliding direction.
N number of springs in the bi-stable mechanism.
k_b stiffness of the spring in the bi-stable mechanism.
L_0 free length of the spring in the bi-stable mechanism.
L actual length of the spring in the bi-stable mechanism.
H distance between the upper revolute joint of the spring and the sliding path.
x position of the end-effector with respect to the neutral position of the springs in the bi-stable mechanism.
C total stroke of the bi-stable mechanism.
C_1 distance between the neutral position of the springs in the bi-stable mechanism and the forward end-stop.
C_2 distance between the neutral position of the springs in the bi-stable mechanism and the back end-stop.
x_t coordinate of the end-effector.
m_t mass of the end-effector.
L_t length of the end-effector.
k_c equivalent stiffness of the collision between the end-effector and the obstacle.
χ_c hysteresis coefficient of the collision between the end-effector and the obstacle.
e_c coefficient of restitution of the collision between the end-effector and the obstacle.
k_{be} equivalent stiffness of the collision between the end-effector and the back end-stop.

χ_{be} hysteresis coefficient of the collision between the end-effector and the back end-stop.
e_{be} coefficient of restitution of the collision between the end-effector and the back end-stop.
k_{fe} equivalent stiffness of the collision between the end-effector and the forward end-stop.
c_{fe} equivalent damping coefficient of the collision between the end-effector and the forward end-stop.
F_e force generated by the impact with an end-stop.
x_o position of the obstacle.
a_c acceleration imposed by the robot control system.
d_c deceleration imposed by the robot control system.
V_c maximum velocity of the robot in the trapezoidal velocity profile.

1 Introduction

In robotics, the risk of collisions is an important issue when the robot does not carry out repetitive tasks and moves in unknown environments.

In recent years, a significant research effort has been made in the field of collision avoidance due to the quick development of collaborative [1] and autonomous robots [2] by the industries. The former must move accordingly to operator safety, whereas the latter can act in unforeseeable ways due to wrong predictions. In both cases, unpredictable collisions must be handled. Thus, the system must be able to detect, or even predict, them and consequently act. Methods and algorithms [3,4,5] have been developed to overcome this issue, making the correct execution of the tasks possible.

However, independently from the considered task, if collisions can happen, the velocity of the robot must be limited, and the efficiency of the system will be penalized. Furthermore, the delay in the communication channel worsens the impacts because no action is taken during this time.

This is particularly relevant in the field of teleoperation. Here, when the delay is not considered, collisions can generate instability that can have disruptive consequences (both for the robot and for the system on which it acts). Different studies have been made [6] and various algorithms have been developed [7] to guarantee optimal behavior and reduce the risk of instabilities.

Many researchers have developed technologies for the mitigation of the effect of hard collisions, developing compliant coverings of the links, back-drivable transmissions, elastic transmissions that are able to decouple joint actuator inertia from link inertia [8], and end- effector air-bags [9].

Mechanisms to mitigate collisions at end effector level are already present on the market in the form of compensation units that are placed between the end effector and the robot flange. However, they are used to compensate for small misalignments in the position of the objects to be picked up. Therefore, their movement is limited.

This paper focuses on the end-effector and deals with the development of a specific compliant mechanism that decouples the tool movement from the robot movement [10]. This mechanical approach exploits a non-linear coupling system to delay the instant in which the robot starts to directly push the impacted object. In this way, the delay in the communication is masked by the decoupled movement of the tool. Hard contacts with surfaces will be softened and the robot has the time to stop or, at least, slow down and reduce the effects of impacts. This solution eliminates the need of limiting the velocity of the robot and the overall performance is increased.

The introduction of passive compliance in a robotic system has to cope with two opposite requirements: on the one hand compliance has to mitigate the consequences of unexpected collisions between the end-effector and an obstacle, on the other hand the robot has to be stiff enough to follow a specific trajectory or perform a precise positioning. Therefore, the end-effector has to be characterized by a variable stiffness, in order to satisfy these two opposite goals.

The use of a linear spring embedded between the robot flange and the end-effector represents a passive compliant mechanical system which increases the compliance and reduces the reflected inertia at the interaction between the end-effector of the robot and the environment. However, the compliance and the equilibrium position cannot be adjusted when linear springs are selected, whereas the use of non-linear springs allows to control both the compliance and the equilibrium position [11, 12].

The novel end-effector introduced in this paper is based on a bi-stable mechanism. The term bi-stable refers to systems characterized by two stable equilibrium positions. This mechanism represents a passive adjustable compliant system which acts as a non-linear spring and introduces the following advantages over the linear spring:

- the force applied on the obstacle during the interaction gradually decreases when the compression of the non-linear spring increases. This prevents overloading the robot and the obstacle when the pre-load is exceeded;
- the second position of stability of the bi-stable mechanism allows to detach the end-effector from the obstacle, interrupting the interaction. This is very important when the interaction has to be interrupted as soon as possible to preserve the integrity of the obstacle or the end-effector.

The main limit of the proposed end-effector is that it is not able to protect the robot from possible collisions of the links with obstacles in the workspace.

The paper is organized as follows.

The mathematical model of the robot equipped with the novel end-effector is presented in Section 2 and numerical results are presented in Section 3 to show the behavior of the end-effector. In Section 4, design parameters and operating conditions are analyzed to state their influence on the performance of the end-effector. Finally, in Section 5 the numerical model is validated by means of experimental tests carried out on a prototype.

2 Mathematical model

The aim of the mathematical model is to estimate the effects of accidental collisions on the end-effector and the

Journal of Mechanical Design. Received May 31, 2021;
Accepted manuscript posted September 01, 2021. doi:10.1115/1.4052443

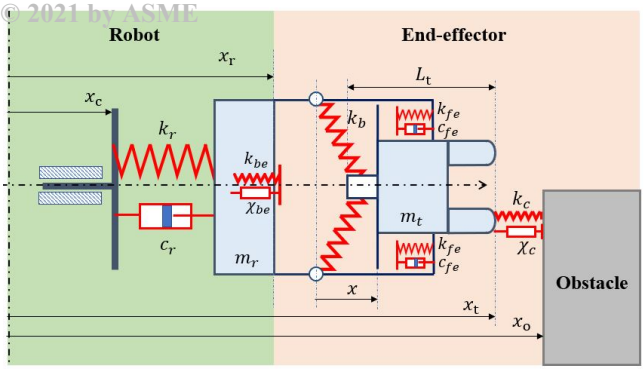

Fig. 1: Lumped parameter model of the interaction between the robot, the end-effector and the obstacle

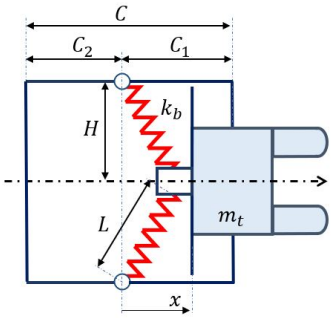

Fig. 2: Geometric model of the bi-stable mechanism. C is the total stroke. In the first part (C_1) of the total stroke the bi-stable mechanism generates a positive force, in the second part (C_2) the bi-stable mechanism generates a negative force

robot. The mathematical model simulates the behavior of the robotic system in the approach direction. The full model, which is represented in Figure 1, consists of three sub-models: the robot, the end-effector and the obstacle. The analysis assumes a one-dimensional model of the collision, hence only planar movements of the robot are considered. In these hypotheses, the multi-degree of freedom (DOF) model of the robot is reduced to a one-dimensional model, represented by a base excited mass-spring-damper system. The aim of this model is to consider the inertia and compliance of the robot along the approach direction. The mechanical properties of the robot were identified by means of impulsive modal analysis [13, 14], then, the measured properties were reduced to the trajectory of the robot flange in the Cartesian space [15].

The lumped parameters m_r, k_r and c_r represent the reduced mass, stiffness and damping of the robot, respectively. Coordinate x_c represents the motion law of the robot flange imposed by the control system, i.e., the motion of the robot flange which is generated by the robot with ideal motors, without compliances and clearances. The coordinate x_r represents the actual motion of the robot flange, accounting for the inertia and the compliance of the robot. The end-effector, schematized through the mass m_t, is connected to the robot flange by means of a bi-stable mechanism.

Bi-stable mechanisms are widely used in micromechanics, space and energy harvesting applications for their unique properties [16], [17], [18]. Bi-stable mechanisms are mechanical systems equipped with flexible elements (springs, membranes or foils) which have two stable equilibrium positions separated by an un-stable equilibrium position. When the mechanism in a stable equilibrium position is stimulated by an external force, first the elastic elements deflect and store energy, then, after the un-stable equilibrium position is reached, the stored energy is released and the system is attracted towards the second stable equilibrium position.

The bi-stable mechanism considered in this analysis is represented in Figure 2. It is a chevron-type mechanism [16] and is equipped with two simple linear springs connected to a sliding element, which is constrained to move along the x-axis.

The component F_b of the force generated by the springs

Parameter	Unit	Value
N	/	2
k_b	Nm^{-1}	200
H	m	0.03
C	m	0.03
C_1	m	0.015
C_2	m	0.015
L_0	m	0.05

Table 1: Reference values of the parameters of the bi-stable mechanism (Figure 2)

of the bi-stable mechanism in the sliding direction is:

$$F_b = N k_b (L_0 - L)\frac{x}{L} \tag{1}$$

$$L = \sqrt{H^2 + x^2} \tag{2}$$

In the configuration of Figure 1 and 2 the spring forces perpendicular to sliding direction cancels out and no net force is transmitted to the robot in this direction.

The geometric parameters assumed for the bi-stable mechanism are listed in Table 1, and the force F_b as a function of the ratios (x/L_0) and (H/L_0) is represented in Figure 3.

Figure 3 shows that the bi-stable mechanism generates a positive force in the first portion C_1 of the total stroke C. On the contrary, the generated force is negative in the latter portion C_2, which means that the mass m_t spontaneously moves backwards, towards the second stable position. The impact between the mass m_t of the end-effector and the obstacle is schematized by means of an elastic element and a damping element in parallel, see Figure 1. The contact force depends on the deformation $\delta = (x_t - x_o)$ and the deformation velocity $\dot{\delta} = \dot{x}_t$, where x_t is the coordinate of the end-effector and x_o is the position of the obstacle in the cartesian space.

Journal of Mechanical Design. Received May 31, 2021;
Accepted manuscript posted September 01, 2021. doi:10.1115/1.4052443

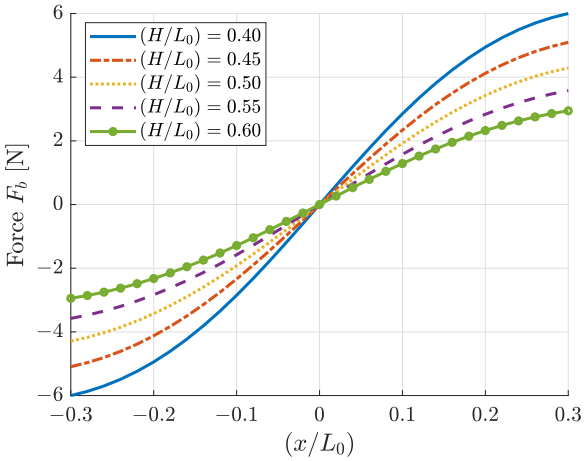

Fig. 3: Force F_b as a function of the rations (x/L_0) and (H/L_0), with the parameters of Table 1

The contact force is formulated according to this equation [19]:

$$F_c = k_c\delta^m + \chi_c\delta^n\dot{\delta} \tag{3}$$

where exponents m and n are set to $m = n = 3/2$, in agreement with Hertz contact law [19]. The constant χ_c is defined referring to the model proposed in [20]:

$$\chi_c = \frac{3}{2}\frac{(1-e_c)}{e_c}k_c\frac{1}{\dot{\delta}_{in}} \tag{4}$$

where e_c is the coefficient of restitution of the impact [21] and $\dot{\delta}_{in}$ is the initial relative velocity of the impact. The equations of motion of robot and end-effector during the collision are:

$$m_r\ddot{x}_r = c_r(\dot{x}_c - \dot{x}_r) + k_r(x_c - x_r) - F_b \tag{5}$$
$$m_t\ddot{x}_t = F_b - k_c\delta^m - \chi_c\delta^n\dot{\delta} \tag{6}$$

They are non-linear owing to the formulations of the contact force and of mechanism force. Equation 5 shows that the force exerted on the robot is F_b , which can be calculated from equation 6 that represents the dynamic equilibrium of the end-effector.

The movement of the slider of the end-effector, inside the bi-stable mechanism, is restricted by the robot flange on one side and by a mechanical constraint on the other side. In order to simulate the contact between the slider and these end-stops, each constraint is modelled by means of an elastic element in parallel with a damping element. The end-stop on the robot flange uses the same formulation of Equations 3 and 4. It activates when $|x| > C_2$ and physically represents a layer of elastomeric material with equivalent stiffness k_{be} and coefficient of restitution e_{be}. The other end-stop is modelled using a simple linear spring-damper system. This approach reduces the computational effort of the simulation. This end-stop consists in a layer of elastomeric material, with an equivalent contact stiffness k_{fe} and damping coefficient c_{fe} (Figure 1). It activates when $x > C_1$.

When an end-stop is impacted the equations of motion become:

$$m_r\ddot{x}_r = c_r(\dot{x}_c - \dot{x}_r) + k_r(x_c - x_r) - F_b - F_e \tag{7}$$
$$m_t\ddot{x}_t = F_b - k_c\delta^m - \chi_c\delta^n\dot{\delta} + F_e \tag{8}$$

where F_e represents the contact force due to the impact with an end-stop. F_e is given by:

$$F_e = k_{be}(|x| - C_2)^m + \chi_{be}(|x| - C_2)^n|\dot{x}| \tag{9}$$

when the end-effector impacts with the back end-stop. F_e is given by:

$$F_e = -k_{fe}(x - C_1) - c_{fe}\,\dot{x} \tag{10}$$

when the end-effector impacts with the forward end-stop.

3 Numerical Simulations

The mathematical model of Figure 1 was implemented in MATLAB/Simulink, which is suited to carry out non-linear simulations. Simulations are aimed to verify that the bi-stable mechanism is able to mitigate the contact force and the force on the robot when an accidental collision occurs. To verify the effectiveness of the bi-stable mechanism, two cases are considered:

1. the end-effector is rigidly fastened on the robot flange. In this case the bi-stable mechanism is not adopted and the mass m_t of the end-effector is added to the reduced mass m_r of the robot;
2. the bi-stable mechanism is mounted between the end-effector and the robot flange.

The robot considered in this analysis is the Omron Adept Viper s650. Simulations assume a generic operation of the robot, in which the end-effector is initially stationary and moves towards a target position along a linear trajectory. A trapezoidal velocity profile with acceleration a_c and deceleration d_c is assumed. An accidental collision occurs between the end-effector and an obstacle, when the robot is moving at a constant velocity V_c.

It is assumed that the robot stops when the impact with the obstacle is detected. The impact sensor of the end-effector equipped with the bi-stable mechanism is an inductive sensor. This sensor switches on when the end-effector moves of 5 *mm* from the forward end-stop. When the end effector is rigidly fastened to the robot, the collision is detected by means of a force sensor embedded in the end-effector, which switches on when the force overcomes 25 *N*.

Journal of Mechanical Design. Received May 31, 2021;
Accepted manuscript posted September 01, 2021. doi:10.1115/1.4052443

Parameter	Unit	Value
a_c	ms^{-2}	1
d_c	ms^{-2}	2
m_t	kg	0.75
k_c	$Nm^{-1.5}$	10^8
e_c	/	0.65
k_{be}	$Nm^{-1.5}$	10^6
e_{be}	/	0.6
k_{fe}	Nm^{-1}	10^6
c_{fe}	Nsm^{-1}	278
DT	s	$16 \cdot 10^{-3}$

Table 2: Reference values of the parameters assumed in the simulations

Parameter	Unit	Value
q	°	[0; -87; -105; 0; -78; 0]
m_r	kg	8.4
k_r	Nm^{-1}	$2.3 \cdot 10^5$
c_r	Nsm^{-1}	71

Table 3: Values of the parameters correlated to the robot configuration **q** in the joint space just before the collision

When the interaction between the end-effector and the obstacle is analyzed, three events take place: the collision, in which the contact begins; the detection of the collision, when the impact detector is switched on; the reaction, when the robot brakes. It is assumed that the reaction does not coincide with the detection, since the time needed by the robot control system to process the external input from the sensor is considered. External inputs are updated at every *scan cycle*, which is a specific feature of the robot. In the worst case, when the input signal switches on after being requested by the control system, it is necessary to wait a full scan cycle to detect it. Hence, the scan cycle represents the maximum time needed to process the external signal. The difference between the detection and the reaction is defined as *dead time DT*. In this analysis the dead time is assumed coincident with the scan cycle of the robot. The difference between the instant in which the collision begins and the instant in which the robot brakes is defined as *reaction time* t_r.

The values of the parameters adopted in the simulations are listed in Table 2.

The configuration **q** of the robot in the joint space just before the collision and the related reduced mass m_r, stiffness k_r and damping c_r are reported in Table 3.

Figure 4a represents the velocity profiles $\dot{x}_c$, $\dot{x}_r$ and $\dot{x}_t$ when the end-effector is rigidly fastened on the robot flange. Figure 4b represents the corresponding contact force generated in the collision between the end-effector and the obstacle. For the sake of simplicity, the contact force applied on the end-effector is represented in Figure 4b as a positive force, although it is negative in the mathematical description. It is worth noticing that, in this case, the contact force coincides with the force which directly excites the robot. Robot flange velocity is $V_c = 0.05\ ms^{-1}$.

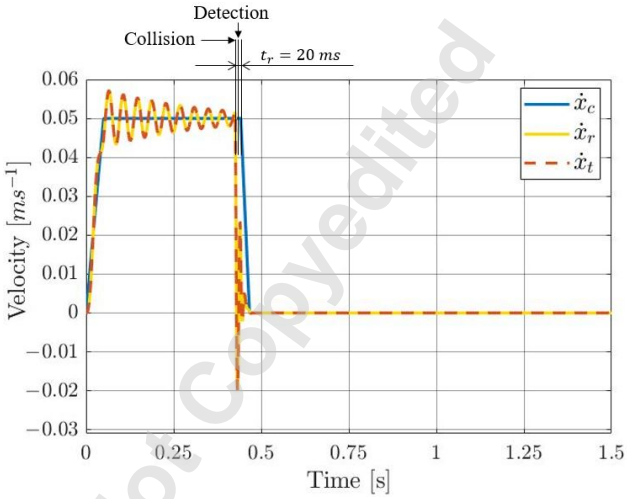

(a)

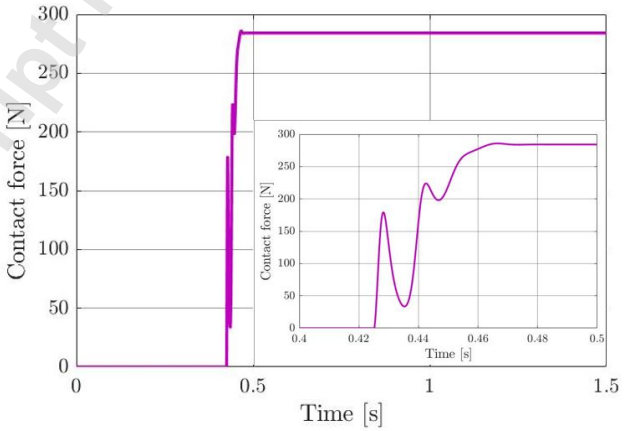

(b)

Fig. 4: End-effector rigidly fastened on the robot flange: (a) velocity profiles; (b) contact force profile. Parameters of the simulation are listed in Table 2

The velocity of the robot mass is characterized by a damped oscillation when the robot reaches V_c, since the spring and the damper, which represent the mechanical properties of the robot, are compressed during the acceleration phase. The collision between the end-effector and the obstacle causes the sudden deceleration of the robot mass. However, since the reaction time of the robot is not fast enough, the motors of the robot keep running. The collision, detection and reaction of the robot are highlighted in Figure 4a. The detection occurs in 4 *ms*, whereas the reaction time t_r is 20 *ms*. The contact force profile in Figure 4b reveals that the

Journal of Mechanical Design. Received May 31, 2021;
Accepted manuscript posted September 01, 2021. doi:10.1115/1.4052443

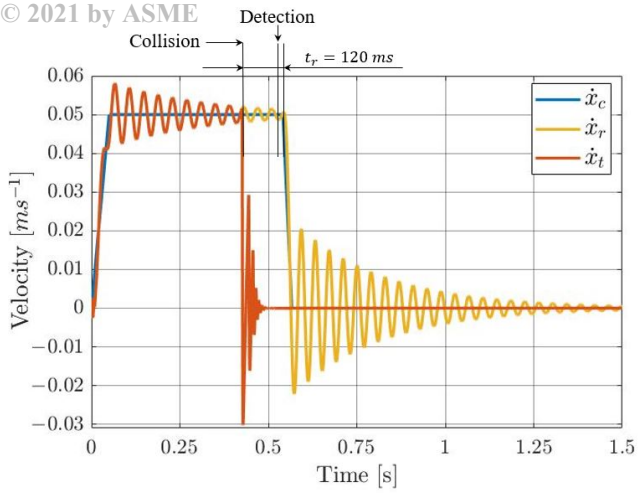

(a)

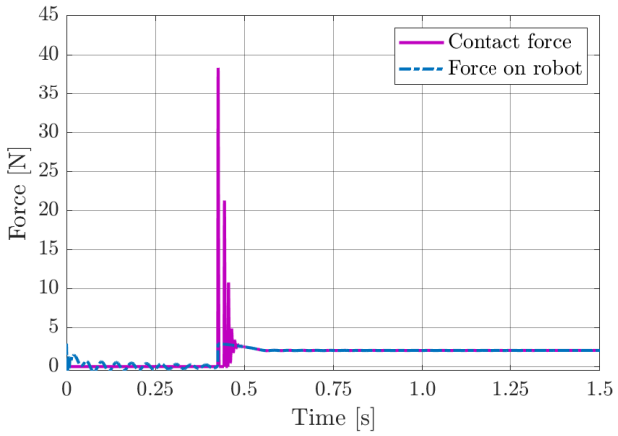

(b)

Fig. 5: End-effector with bi-stable mechanism: (a) velocity profiles; (b) profiles of the contact force and the force on the robot. Parameters of the simulation are listed in Table 1 and 2

robot deforms, as the contact force increases far beyond the force threshold of 25 N.

Figure 5a represents the velocity profiles $\dot{x}_c$, $\dot{x}_r$ and $\dot{x}_t$ when the bi-stable mechanism is adopted. Figure 5b represents the contact force generated in the collision between the end-effector and the obstacle, and the force applied on the robot. For the sake of simplicity, the contact force and the force on the robot are represented in Figure 5b as positive forces, although they are negative in the mathematical description. It is worth noticing that in this case the contact force does not coincide with the force which directly excites the robot. The parameters of the simulation are listed in Table 1 and 2. Robot flange velocity is $V_c = 0.05\ ms^{-1}$.

Figure 5a highlights that the force generated by the bi-stable mechanism is enough to counterbalance the force of inertia acting on the end-effector and, before the collision, the end-effector moves with the robot. The collision causes a sudden deceleration of the end-effector, while the robot mass is moving forward smoothly. It is worth noticing that the reaction time t_r of the robot with the bi-stable mechanism ($t_r = 120\ ms$) is longer than the one of the robot with rigidly fastened end-effector ($t_r = 20\ ms$). Actually, the end-effector takes more time to move of 5 mm from the forward end-stop than the contact force to rise up to 25 N. The time needed to detect the collision is an important parameter that has to be taken into account in the design of such mechanisms. The increase in the reaction time requires larger decoupling distance, hence a longer stroke of the mechanism. In Figure 5a the bi-stable mechanism allows to decouple the movement of the robot from the movement of the end-effector, because the robot mass does not change its velocity during collision, but only when the impact is detected and the robot brakes. After braking the robot oscillates because it is not in direct contact with the obstacle.

Figure 5b highlights that the end-effector bounces many times on the obstacle. The robot equipped with the bi-stable mechanism reduces the contact force by about 85%.

The decoupling between the end-effector and the robot absorbs the collision, preventing that the large inertia and stiffness of the robot are involved in the collision.

In the case analysed in Figure 5 the end-effector does not cross the neutral position of the spring in the bi-stable mechanism, since after the collision end-effector velocity with respect to the robot ($\dot{x}_t$- $\dot{x}_r$) does not show a negative mean value corresponding to the attraction towards the second equilibrium position. Therefore, the bi-stable mechanism behaves as a spring with variable stiffness. In this condition the maximum force applied to the robot coincides with the maximum force generated by the springs of the bi-stable mechanism, since there is no impact with the back end-stop.

However, if the end-effector crosses the neutral position of the system ($x = 0$), the end-effector moves towards the robot flange and a collision occurs when the end-effector reaches the end-stop. This behavior is highlighted in Figure 6a, which represents the velocity profiles $\dot{x}_c$, $\dot{x}_r$ and $\dot{x}_t$, assuming a velocity of the robot ($V_c = 0.25\ ms^{-1}$) larger than the one of Figure 5. Figure 6b represents the corresponding contact force and total force on the robot.

Figure 6a shows that after the collision the velocity of the end-effector becomes negative, then it increases as $F_b > 0$ in the first portion of the stroke. When the neutral position of the spring ($x = 0$) is crossed the velocity of the end-effector decreases, until the back end-stop is reached.

Actually, after the collision the negative mean value of end effector velocity with respect to the robot corresponds to the attraction towards the second equilibrium position.

Figure 6b shows that the contact force has a single peak, as the end-effector directly moves towards the robot flange after the collision with the obstacle. The change in the sign of the robot force highlights the passage through the neutral position of the bi-stable mechanism. The force on the robot is characterized by several peaks, due to multiple bouncing of the end-effector on the back end-stop. However, the force applied on the robot is much smaller than the contact force. In this case the reaction time t_r is shorter than in the previous case, as the higher velocity V_c and contact force reduce the time needed by the end-effector to move away from the forward end-stop. It is worth noticing that the mechanism

Journal of Mechanical Design. Received May 31, 2021;
Accepted manuscript posted September 01, 2021. doi:10.1115/1.4052443

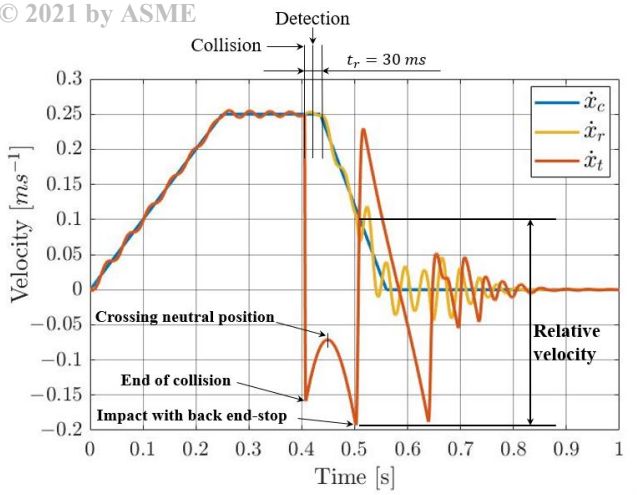

(a)

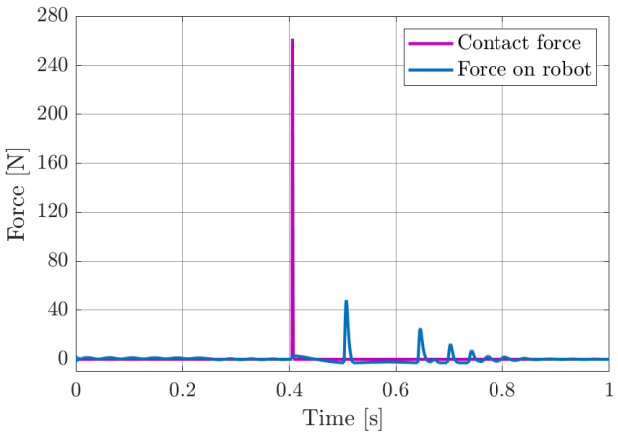

(b)

Fig. 6: End-effector with bi-stable mechanism: (a) velocity profiles; (b) profiles of the contact force and the force on the robot. Parameters of the simulation are listed in Table 1 and 2

allows to decouple the end-effector from the robot only if the stopping distance of the robot is shorter than the total stroke of the system. If this condition is not fulfilled, a second collision occurs and this time the inertia and the stiffness of the robot are involved, as the end-effector is laying directly against the robot flange.

4 Parametric analysis of the mechanism

In the mitigation of an accidental collision, the main goals are:

- minimization of the contact force, to prevent damages of the end-effector;
- minimization of the force applied to the robot, as the robot is very expensive to repair or replace.

This section analyses the effects of different parameters on the contact force and the force applied on the robot.

The parameters of the simulations listed in Tables 1 and 2 refer to end-effector properties corresponding to general purpose grippers and to impact with hard obstacles, which can be found in the industrial environment.

4.1 Effect of parameters on contact force

In the collision of two masses, the contact force mainly depends on the momentum of the masses, just before the collision, and on the contact stiffness k_c [21]. The decrease in the mass of the end-effector allows the robot to move at higher velocity, without increasing the contact force due to accidental collisions.

Figure 7 shows the maximum value of the contact force as a function of the mass m_t and the velocity of the robot V_c.

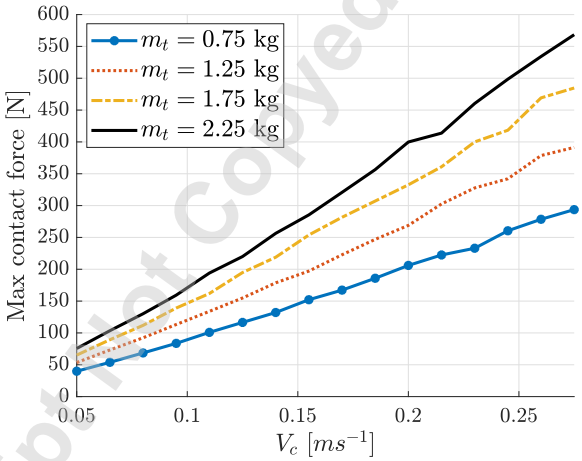

Fig. 7: Maximum value of contact force as a function of robot velocity V_c and end-effector mass m_t

The contact force increases almost linearly as a function of the velocity of the robot, considering a certain mass m_t.

The reduction in the contact stiffness decreases the maximum value of the contact force, allowing to increase the velocity of the robot. Figure 8 represents the maximum value of the contact force as a function of velocity V_c and contact stiffness k_c.

The increase in k_b leads to a slightly increase in the peak of the contact force. Figure 9 represents the peak value of the contact force as a function of the velocity of the robot V_c and the stiffness k_b of the bi-stable mechanism.

The *dead time DT* is related to the effect of the robot control system on the interaction between the robot, the end-effector and the obstacle. Figure 10 represents the maximum value of the contact force as a function of the velocity of the robot V_c and the dead time DT.

The maximum value of the contact force is independent from the time delay DT. It is worth noticing that this result holds true when the total stroke of the mechanism C is larger than the stopping distance. On the contrary, a collision between the robot flange and the obstacle occurs. Actually, the stroke of the bi-stable mechanism is just enough to decouple the end-effector from the robot for $V_c = 0.25\ ms^{-1}$ and $DT = 0.05\ s$. In these conditions, the robot flange reaches

Journal of Mechanical Design. Received May 31, 2021;
Accepted manuscript posted September 01, 2021. doi:10.1115/1.4052443

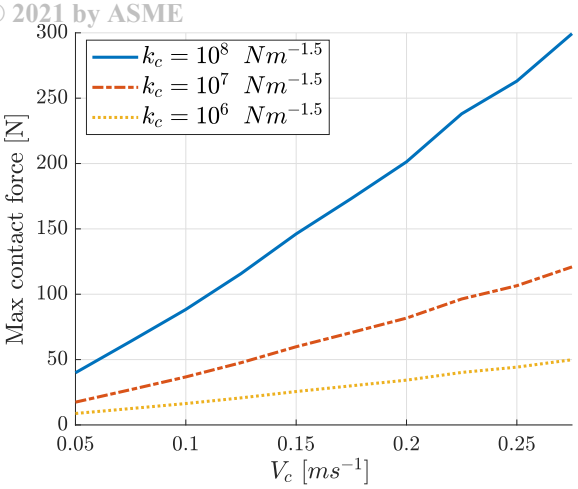

Fig. 8: Maximum value of contact force as a function of robot velocity V_c and contact stiffness k_c

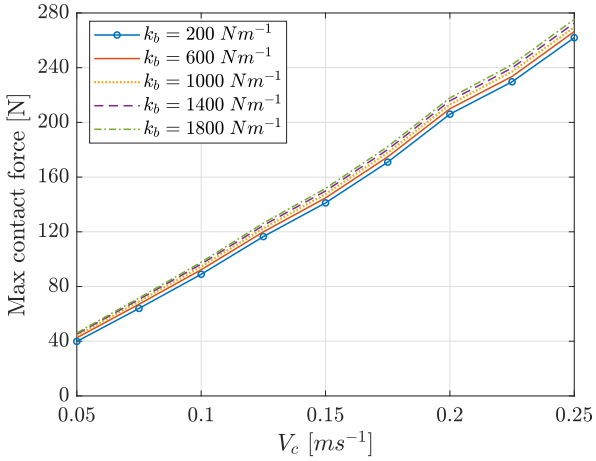

Fig. 9: Maximum value of contact force as a function of robot velocity V_c and stiffness k_b of the bi-stable mechanism

the obstacle, but a small collision occurs, as the robot has already reduced its velocity. This small collision is highlighted by the peak in the upper right corner in Figure 10.

4.2 Effect of parameters on the force applied on the robot

The end-effector moves towards the robot flange up to reach the end-stop when it crosses the neutral position of the bi-stable mechanism ($x = 0$). The force on the robot caused by the collision between the end-effector and the end-stop depends not only on the mechanical properties of the end-stop and on the momentum of the end-effector before the collision, but also on the dynamics of the robot after the collision. Figure 11 represents the maximum force on the robot as a function of the velocity V_c and the mass m_t. Figure 11 allows to define three main scenarios:

1. the end-effector does not impact with the back end-stop;
2. the end-effector impacts with the back end-stop after the robot stop;

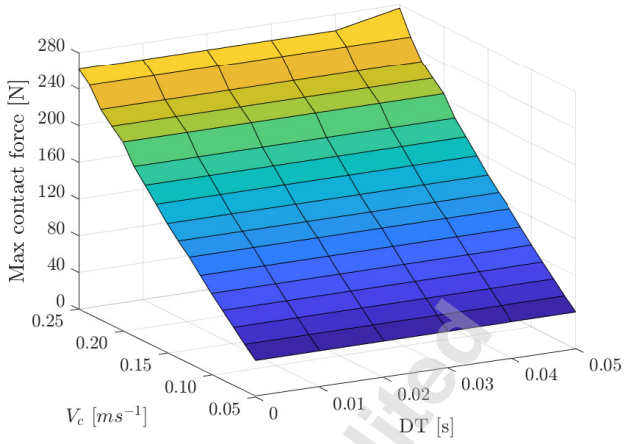

Fig. 10: Maximum value of contact force as a function of robot velocity V_c and dead time DT

3. the end-effector impacts with the back end-stop before the robot stop.

The three scenarios highlighted in Figure 11 refers to the end-effector with $m_t = 0.75 \ kg$.

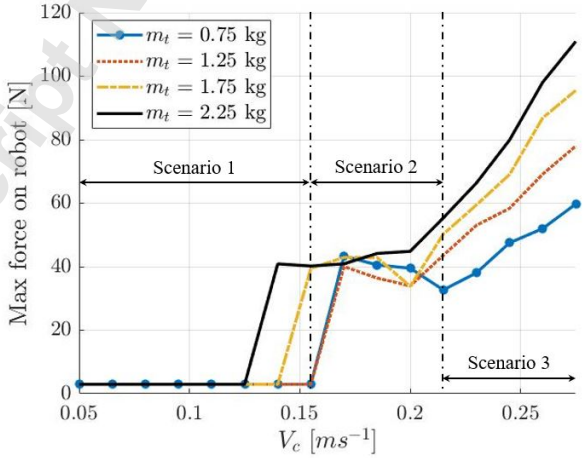

Fig. 11: Maximum value of the force on robot as a function of robot velocity V_c and end-effector mass m_t

The first scenario, which is depicted in Figure 5, is characterized by the smallest value of the force on the robot, since the contact force is not enough to move the end-effector beyond the neutral position of the springs.

In the second scenario the increase in the contact force is enough to move the end-effector beyond the neutral position of the springs. Hence, the force on the robot significantly increases, due to the collision of the end-effector with the back end-stop. It is worth noticing that the second scenario represents a transition phase, in which the non-linear interaction between the robot, the end-effector and the obstacle is also affected by the inertia force, due to the braking of the robot. Figure 12 represents the velocity profiles $\dot{x}_c$, $\dot{x}_r$ and $\dot{x}_t$, as-

suming a velocity of the robot $V_c = 0.20\ ms^{-1}$, which refers to scenario 2.

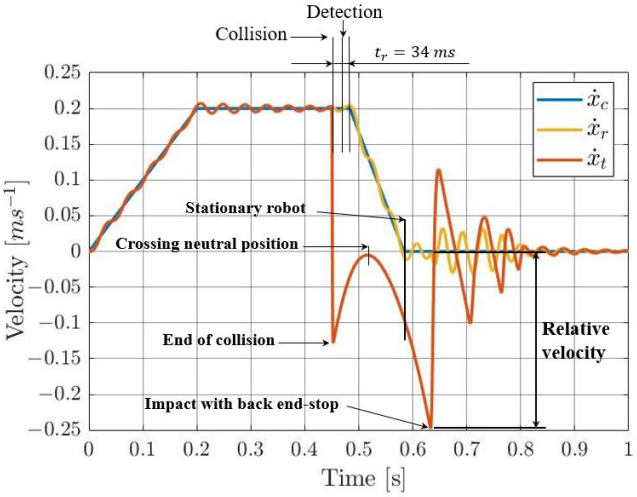

Fig. 12: End-effector with bi-stable mechanism: velocity profiles in scenario 2 ($V_c = 0.20\ ms^{-1}$, $m_t = 0.75\ kg$). Parameters used in the simulation are listed in Table 1 and 2

Figure 12 highlights that the collision between the end-effector and the back end-stop occurs when the robot is stationary. The relative velocity between the robot and the end-effector is smaller in Figure 12 than in Figure 6, causing a smaller force on the robot. It is worth noticing that in Figure 6 the end-effector moves towards the robot flange only when the robot is braking, whereas in Figure 12 a portion of the movement of the end-effector occurs when the robot is stationary. This behavior affects the maximum negative velocity reached by the end-effector before impacting with the back end-stop, hence the relative velocity of impact. The direct comparison between the velocity of the end-effector in the scenarios of Figures 6 and 12 is represented in Figure 13.

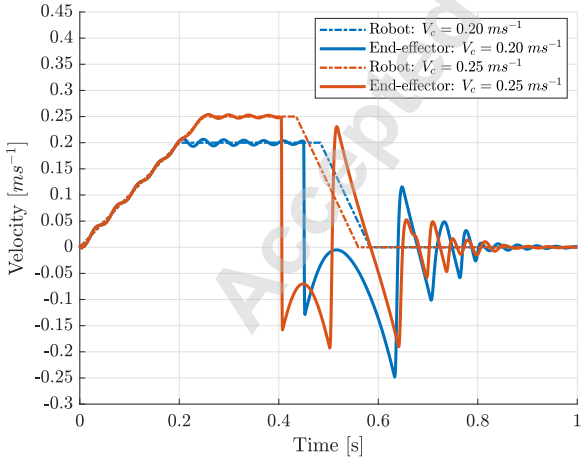

Fig. 13: Comparison between the velocity of the end-effector for $V_c = 0.20\ ms^{-1}$ and $V_c = 0.25\ ms^{-1}$ (Scenarios 2 and 3, respectively)

In the third scenario, which is reproduced in Figure 6, the force on the robot increases with the velocity of the robot and the mass of the end-effector. The impact velocity increases for higher velocity of the robot, as the robot takes more time to decelerate.

The force on the robot as a function of the velocity of the robot V_c and the dead time DT is represented in Figure 14. Figure 14 corroborates the existence of three working modes of the end effector. The bi-stable behavior does not occur when the velocity V_c and dead time are small. The end-effector collides with the back end-stop for higher velocities and dead times.

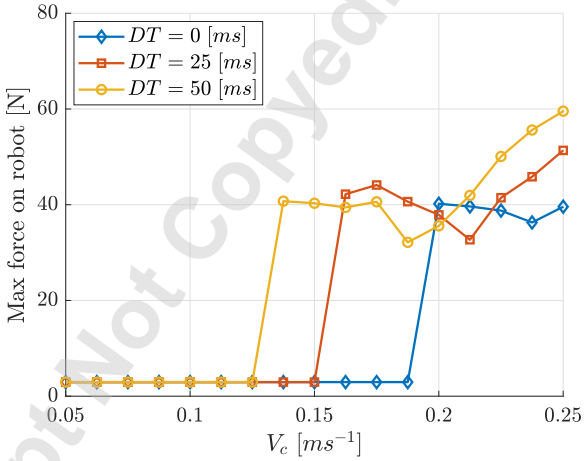

Fig. 14: Maximum value of the force on robot as a function of robot velocity V_c and dead time DT, $m_t = 0.75\ kg$

5 End-effector design and validation

A prototype end-effector equipped with the bi-stable mechanism was developed, in order to validate the presented mathematical model. The sorting of small components in bulk, by means of a teleoperated robot, is the task considered to define the features of the end-effector. In this scenario accidental collisions against obstacles can occur, when the operator makes mistakes. Hence, the tool of the end-effector consists of a paddle, which is used to push the small components in the working plane.

In the design of the bi-stable mechanism three aspects have to be considered:

- a lightweight end-effector is needed to keep small the contact force in all three working scenarios of the bi-stable mechanism;
- the moment of inertia of the end-effector around the rotation axis of the sixth joint (see Figure 15b) has to be as small as possible. The rotation of the sixth joint can quickly reset the end-effector for a new task, exploiting the two stable equilibrium positions;
- sometimes it is hard to find springs with low stiffness.

Journal of Mechanical Design. Received May 31, 2021;
Accepted manuscript posted September 01, 2021. doi:10.1115/1.4052443

These observations led to the design of the bi-stable mechanism with one spring, unlike it was represented in Figures 1 and 2, and the spring was placed horizontally, so that it does not interfere with the movements of the robot. Figures 15a and 15b represent the CAD model of the end-effector and the built prototype, respectively.

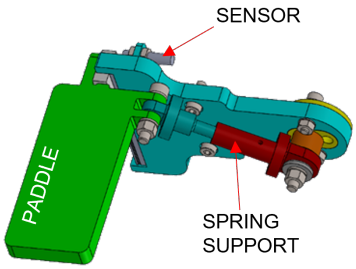

(a)

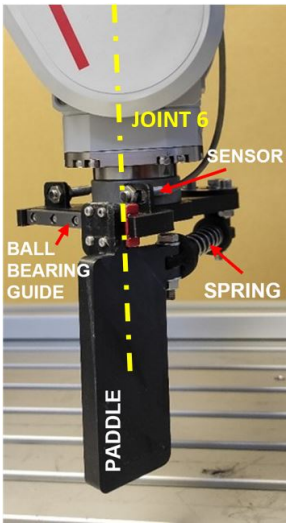

(b)

Fig. 15: Prototype developed for the experimental validation of the models: (a) CAD model; (b) real model.

The main issues related to the design of the end-effector regard friction and clearances between sliding parts, since they can cause sticking phenomena, which increase the risk of locking the slider. Materials with low coefficient of friction have to be selected to reduce friction forces in sliding elements, as PTFE, or, alternatively, ball bearing guides can be used. In the built prototype a ball bearing guide is adopted to guarantee the smooth-sliding of the paddle.

The prototype was built by means of additive manufacturing by using a plastic material (PLA). This manufacturing process allows to realize lightweight components, which is an important aspect in the reduction of the contact force, but some problems have to be highlighted. First, the components of the end-effector can introduce an uncontrollable compliance, if they are not stiff enough, due to the small Young's modulus of the material. Second, it is hard to obtain small dimensional and geometric tolerances. Moreover, the surfaces of the moving components can be very rough. Therefore, the large clearances and the high roughness of the surfaces increase the friction and stick-slip phenomena. In order to consider all possible sources of friction, the mathematical model described by equations 7 and 8 can be updated as follows:

$$m_r\ddot{x}_r = c_r(\dot{x}_c - \dot{x}_r) + k_r(x_c - x_r) - F_b - F_e - F_f \quad (11)$$

$$m_t\ddot{x}_t = F_b - k_c\delta^m - \chi_c\delta^n\dot{\delta} + F_e + F_f \quad (12)$$

where F_f is the friction force acting along the sliding axis of the paddle and it is defined as follows:

$$F_f = \mu\, F_n\, tanh\left(\frac{\dot{x}_r - \dot{x}_t}{v_0}\right) \quad (13)$$

where μ is an equivalent friction coefficient, v_0 is a constant and F_n is the force component generated by the bi-stable mechanism perpendicular to the sliding direction.

$$F_n = N\, k_b\, (L_0 - L)\, \frac{H}{L} \quad (14)$$

The end-effector is equipped with an inductive sensor, which is used to detect when the paddle detaches from the forward end-stop, due to the collision with the obstacle. Such sensor provides a digital signal once the paddle has slid of 1.5 *mm* from the forward end-stop.

5.1 Experimental validation

A series of experimental tests were performed in order to validate the mathematical model. The end-effector is moved by the robot towards an obstacle, following a linear trajectory with a trapezoidal velocity profile. In order to minimize the risk of robot damages, in the first series of tests a "soft" obstacle made of a polystyrene block was used. Further tests with stiffer obstacles are planned in the next future.

Three white markers are attached to the robot, the paddle, and the obstacle and a high frame rate camera is used to track such markers at $\sim$300 fps, during the interaction between the end-effector and the obstacle. Figure 16 represents a snapshot of the experimental setup, where the black cards are used to eliminate reflections and improve the performance of the tracking system.

The experimental result of a typical tracking and the corresponding simulation can be seen in Figure 17a and 17b. The values of parameters used in the simulation are listed in Table 4. It is worth noticing that the parameters are rather different from the ones on Table 2, since the prototype was built using the available components and manufacturing technology, and the obstacle is made of polystyrene, which reduces the contact stiffness to $k_c = 0.6 \cdot 10^5\ Nm^{-1.5}$, in order to avoid possible damages of the robot and the end-effector.

The experimental velocities show the typical features of scenario 3, since the impact with the back end-stop occurs

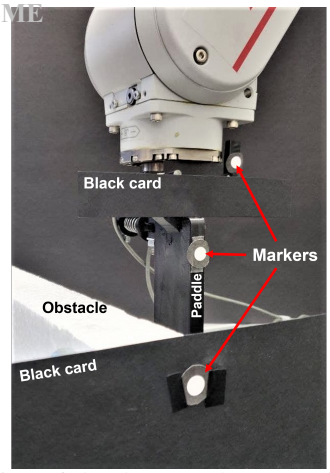

Fig. 16: Position of the three markers: on the obstacle, on the paddle and attached to the robot.

when the robot is still moving. A good agreement between experimental and numerical results is found.

The contact force was validated through the measurement of the acceleration of the end-effector. First, the relation between an impulsive force applied on the tip of the paddle and the acceleration of the paddle was determined. Then, the acceleration during the interaction between the end-effector and the obstacle was measured and an estimation of the contact force was made. To perform these tests an accelerometer (PCB 352C23) was attached to the upper part of the blade, and an impulsive force was exerted on the tip of the paddle by means of an instrumented hammer for modal analysis (PCB086C03), as represented in Figure 18.

The tests showed that the peak force, applied by means of the hammer, and the peak acceleration, measured by means of the accelerometer, are proportional through the mean coefficient $0.564\ Ng^{-1} \pm 0.19\ (95\%)$.

Figure 19a represents the acceleration profile measured with the accelerometer, during the interaction between the end-effector and the obstacle, whereas Figure 19b represents the acceleration profile of the end-effector calculated by means of the numerical model.

Figure 19 highlights that the numerical results are in good agreement with experimental measurements. In the experimental acceleration profiles, the first negative peak, about -6.9 g at 1.08 s, is due to the collision between the end-effector and the obstacle, whereas the first positive peak, about 65.5 g at 1.31 s, is due to the collision between the end-effector and the back end-stop. The comparison with the numerical simulation highlights that the two collisions are well-described. However the experimental tests of Figure 19a show a second negative peak (about -14.5 g, just after the collision with the back end-stop), which is not represented in the simulation of Figure 19b. Actually, the impact force is not applied along the sliding axis of the paddle. Therefore, the torque generated during the interaction can generate an oscillation of the paddle, when the force applied on the paddle is large, and this behaviour is not caught by the numerical model.

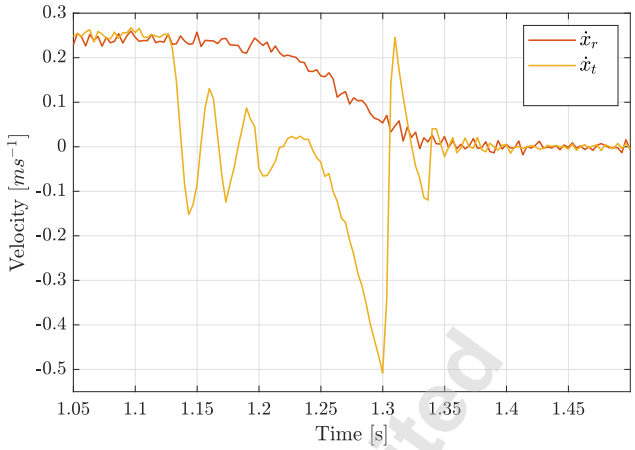

(a)

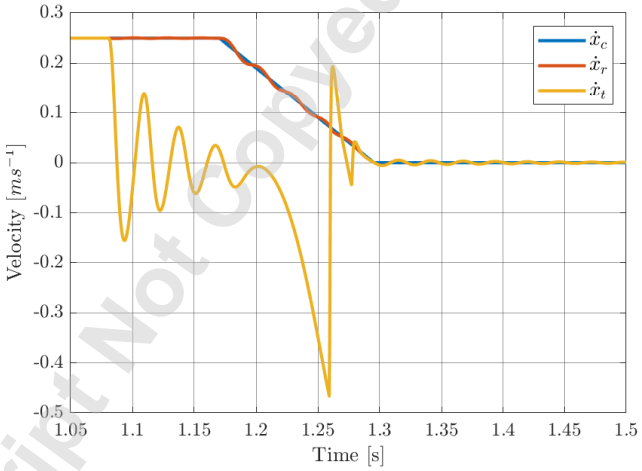

(b)

Fig. 17: Results of tests with the prototype: (a) experimental velocities; (b) simulated velocities. Parameters of the simulation are listed in Table 4

Considering the mean proportionality factor between the force applied on the paddle and the measured acceleration, the experimental acceleration profile allows to estimate the peak in the contact force as follows:

$$max\ contact\ force = 0.564\ (Ng^{-1}) \cdot 6.9\ g = 3.9\ N \quad (15)$$

It is worth noticing that the max contact force is much lower than the one found in Figure 6, because the impacting mass of the end-effector and the contact stiffness are much smaller ($0.048kg$ compared to $0.75kg$ and $0.6 \cdot 10^5\ Nm^{-1.5}$ compared to $10^8\ Nm^{-1.5}$).

Figure 20 represents the absolute value of the contact force during the interaction between the end-effector and the obstacle, calculated by means of the numerical model.

Figure 20 shows that the numerical simulation is in good agreement with the experimentally estimated peak of the contact force.

As can be inferred from Figures 17, 19 and 20 the model can predict the behavior of the end-effector with a good ap-

Parameter	Unit	Value
N	/	1
L_0	m	0.062
k_b	Nm^{-1}	490
H	m	0.053
C	m	0.047
C_1	m	0.0235
C_2	m	0.0235
V_c	ms^{-1}	0.25
a_c	ms^{-2}	1
d_c	ms^{-2}	2
m_t	kg	0.048
k_c	$Nm^{-1.5}$	$0.6{\cdot}10^5$
e_c	/	0.8
k_{be}	$Nm^{-1.5}$	$2.25{\cdot}10^6$
e_{be}	/	0.3
k_{fe}	Nm^{-1}	$2.25{\cdot}10^6$
c_{fe}	Nsm^{-1}	235
DT	s	$70 \cdot 10^{-3}$
μ	/	0.12
v_0	ms^{-1}	0.001

Table 4: Values of the parameters used in the simulations of the real system

proximation, both qualitatively and quantitatively. In particular, a difference of about 5% can be observed in the maximum negative velocity of the end-effector which is influenced by the real friction of the ball bearing guide.

These results are promising and confirm the effectiveness of the end-effector in mitigating the impact of the robot with obstacles.

6 Conclusions

Numerical simulations showed the presence of three working modes of the end-effector with bi-stable mechanism. With low impact speed and short dead time the bi-stable mechanism does not cross the neutral position and a very large reduction in the force applied on the robot is achieved. Then, there is a range of speeds and dead times in which the end-effector crosses the neutral position and impacts the back end-stop, but the impact takes place when the robot is stationary, and a moderate increase in the force on the robot takes place. For large impact velocities the end-effector crosses the neutral position and impacts the back end-stop when the robot is moving. The force on the robot is larger than in the previous cases and depends on the mass of the end-effector. Nevertheless, even in this working mode the bi-stable mechanism strongly reduces the forces with respect to the values that are found with rigid end-effector. Ex-

Fig. 18: Accelerometer and instrumented hammer.

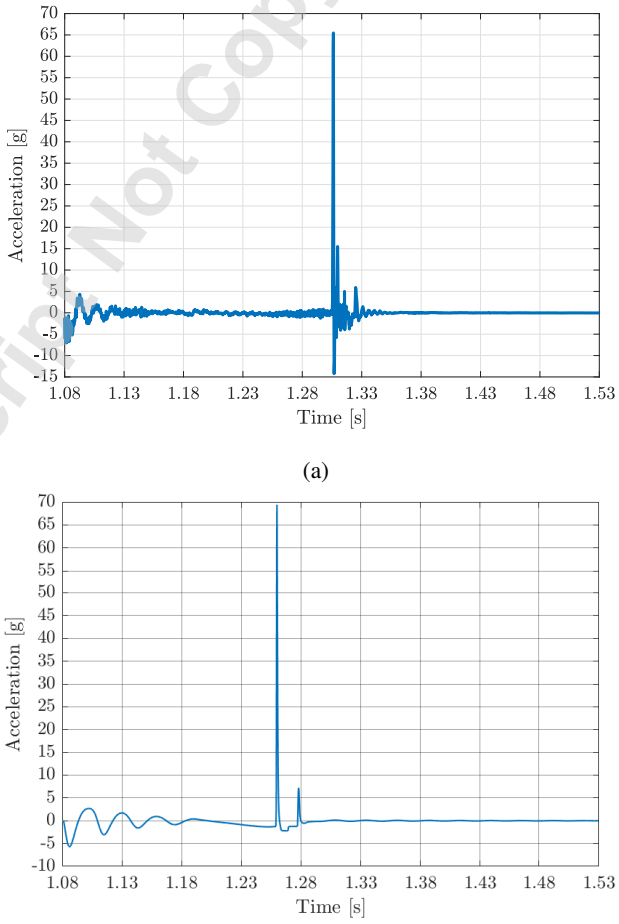

(a)

(b)

Fig. 19: Acceleration profiles: (a) from experimental measurement; (b) from the numerical model.

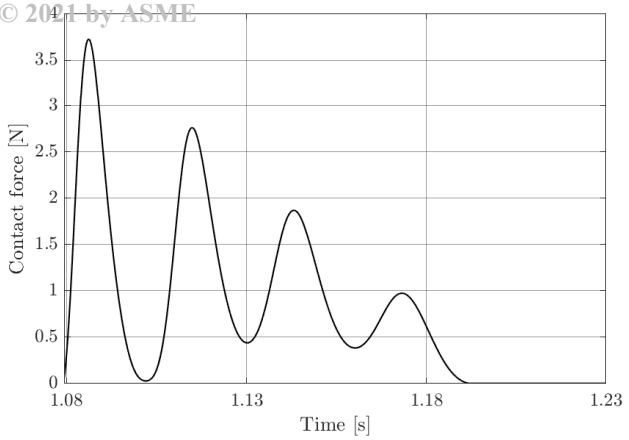

Fig. 20: Contact force profile calculated by means the numerical model. The obstacle is made of soft polystirene.

perimental tests carried out on a prototype impacting on a soft obstacle corroborated the validity of numerical results. It is worth noticing that the novel end-effector has a positive effect on the operating velocity of the robot, since high velocities, that can damage the robot with rigid end-effector in case of collision, can be tolerated if the end-effector with bi-stable mechanism is adopted. The designed bi-stable mechanism has some important advantages with respect to other collision-mitigation technologies. The proposed end-effector can be introduced in existing robots with only minor modifications in the control system. The building of the new end-effector is rather simple and does not require expensive components and sensors. In fact, it is possible to substitute the paddle of the prototype with any other tool (e.g., a gripper for assembly operations) to take advantage of the mitigation of collisions provided by the bi-stable mechanism. According to the envisaged application, the end-effector design can be optimized according to the stiffness of the potential obstacles.

Acknowledgements

This research was funded by University of Padua—Program BIRD 2018—Project no. BIRD187930

References

[1] Boschetti, G., Bottin, M., Faccio, M., and Minto, R., 2021. "Multi-robot multi-operator collaborative assembly systems: a performance evaluation model". *Journal of Intelligent Manufacturing,* **32**(5), pp. 1455–1470.

[2] Cipriani, G., Bottin, M., and Rosati, G., 2021. "Applications of learning algorithms to industrial robotics". *Mechanisms and Machine Science,* **91**, pp. 260–268.

[3] Bottin, M., Boschetti, G., and Rosati, G., 2019. "A novel collision avoidance method for serial robots". *Mechanisms and Machine Science,* **66**, pp. 293–301.

[4] Bottin, M., Rosati, G., and Cipriani, G., 2021. "Iterative path planning of a serial manipulator in a cluttered known environment". *Mechanisms and Machine Science,* **91**, pp. 237–244.

[5] Reyes-Uquillas, D., and Hsiao, T., 2021. "Safe and intuitive manual guidance of a robot manipulator using adaptive admittance control towards robot agility". *Robotics and Computer-Integrated Manufacturing,* **70**, p. 102127.

[6] Lawrence, D. A., 1993. "Stability and transparency in bilateral teleoperation". *IEEE transactions on robotics and automation,* **9**(5), pp. 624–637.

[7] Hokayem, P. F., and Spong, M. W., 2006. "Bilateral teleoperation: An historical survey". *Automatica,* **42**(12), pp. 2035–2057.

[8] Bicchi, A., and Tonietti, G., 2004. "Fast and "soft-arm" tactics [robot arm design]". *IEEE Robotics Automation Magazine,* **11**(2), pp. 22–33.

[9] Weitschat, R., Vogel, J., Lantermann, S., and Höppner, H., 2017. "End-effector airbags to accelerate human-robot collaboration". pp. 2279–2284.

[10] Hannaford, B., and Anderson, R., 1988. "Experimental and simulation studies of hard contact in force reflecting teleoperation". In Proceedings. 1988 IEEE International Conference on Robotics and Automation, IEEE, pp. 584–589.

[11] Ham, R. v., Sugar, T., Vanderborght, B., Hollander, K., and Lefeber, D., 2009. "Compliant actuator designs". *IEEE Robotics & Automation Magazine,* **3**(16), pp. 81–94.

[12] Jujjavarapu, S. S., Memar, A. H., Karami, M. A., and Esfahani, E. T., 2019. "Variable stiffness mechanism for suppressing unintended forces in physical human–robot interaction". *Journal of Mechanisms and Robotics,* **11**(2).

[13] Bottin, M., Cocuzza, S., Comand, N., and Doria, A., 2020. "Modeling and identification of an industrial robot with a selective modal approach". *Applied Sciences,* **10**(13), p. 4619.

[14] Huynh, H. N., Assadi, H., Riviere-Lorphevre, E., Verlinden, O., and Ahmadi, K., 2020. "Modelling the dynamics of industrial robots for milling operations". *Robotics and Computer-Integrated Manufacturing,* **61**, p. 101852.

[15] Tommasino, D., Cipriani, G., Doria, A., and Rosati, G., 2020. "Effect of end-effector compliance on collisions in robotic teleoperation". *Applied Sciences,* **10**(24), p. 9077.

[16] Hwang, I.-H., Shim, Y.-S., and Lee, J.-H., 2003. "Modeling and experimental characterization of the chevron-type bi-stable microactuator". *Journal of Micromechanics and Microengineering,* **13**(6), aug, pp. 948–954.

[17] Zirbel, S. A., Tolman, K. A., Trease, B. P., and Howell, L. L., 2016. "Bistable mechanisms for space applications". *PLOS ONE,* **11**(12), 12, pp. 1–18.

[18] Pellegrini, S. P., Tolou, N., Schenk, M., and Herder, J. L., 2013. "Bistable vibration energy harvesters: A review". *Journal of Intelligent Material Systems and Structures,* **24**(11), pp. 1303–1312.

[19] Hunt, K. H., and Crossley, F. R. E., 1975. "Coefficient of Restitution Interpreted as Damping in Vibroimpact". *Journal of Applied Mechanics,* **42**(2), 06, pp. 440–445.
[20] Hu, S., and Guo, X., 2015. "A dissipative contact force model for impact analysis in multibody dynamics". *Multibody System Dynamics,* **35**(2), pp. 131–151.
[21] Brach, R. M., 2007. *Mechanical impact dynamics: rigid body collisions*. Brach Engineering, LLC.